



Article

Investigating Gravitational Slope Deformations with COSMO-SkyMed-Based Differential Interferometry: A Case Study of San Marco dei Cavoti

Mohammad Amin Khalili ¹, Giuseppe Bausilio ^{1,*}, Chiara Di Muro ¹, Sebastiano Perriello Zampelli ¹ and Diego Di Martire ^{1,2}

¹ Department of Earth Sciences, Environment, and Resources, University of Naples Federico II, Via Cintia 21, 80126 Napoli, Italy; mohammadamin.khalili@unina.it (M.A.K.); chiara.dimuro@unina.it (C.D.M.); sebastiano.perriellozampelli@unina.it (S.P.Z.); diego.dimartire@unina.it (D.D.M.)

² SINTEMA Engineering s.r.l., Viale Maria Bakunin 14, 80126 Napoli, Italy

* Correspondence: giuseppe.bausilio@unina.it

Abstract: Landslides pose significant risks to towns and villages in Southern Italy, including the San Marco dei Cavoti hamlet (Benevento, Campania), where settlements have expanded into areas threatened by landslides, leading to property damage, disruption to the social fabric and loss of life. This study aims to investigate the surface deformations in the area using Differential Interferometry SAR (DInSAR) analysis on COSMO-SkyMed radar imagery and to assess the potential implications for landslide activity. The DInSAR analysis methodology allowed us to obtain high-precision results presented as time series diagrams and maps of cumulative displacement for the study area. Furthermore, the displacement rates derived from the DInSAR analysis were decomposed into vertical and horizontal components to provide better insights into the slope processes and their potential impacts on the San Marco dei Cavoti hamlet. Our significant findings revealed active slope movements and the uphill enlargement of previously inventoried landslides threatening the San Marco dei Cavoti hamlet. These insights contribute to a better understanding of the landslide dynamics in the region and highlight the areas that may require further investigation or intervention measures. In conclusion, this study demonstrates the effectiveness of DInSAR analysis in providing valuable insights into landslide dynamics and informing potential mitigation measures for at-risk communities. This technique could be applied to other landslide-prone regions to support informed decision-making and enhance the safety and resilience of affected communities.

Keywords: slow-moving landslides; mapping and inventory; DInSAR; hazard; San Marco dei Cavoti



Citation: Khalili, M.A.; Bausilio, G.; Di Muro, C.; Perriello Zampelli, S.; Di Martire, D. Investigating Gravitational Slope Deformations with COSMO-SkyMed-Based Differential Interferometry: A Case Study of San Marco dei Cavoti. *Appl. Sci.* **2023**, *13*, 6291. <https://doi.org/10.3390/app13106291>

Academic Editor: José A. Peláez

Received: 22 April 2023

Revised: 18 May 2023

Accepted: 19 May 2023

Published: 21 May 2023



Copyright: © 2023 by the authors. Licensee MDPI, Basel, Switzerland. This article is an open access article distributed under the terms and conditions of the Creative Commons Attribution (CC BY) license (<https://creativecommons.org/licenses/by/4.0/>).

1. Introduction

In Italy, landslides are one of the most dangerous and widespread geohazards, as they often cause loss of human lives and severe economic damage to the social fabric [1–3]. Landslides, defined by Cruden and Varnes [4] as the “movement of a mass of rock, debris or earth down a slope”, are a constant threat to towns and villages in Southern Italy [5,6], where settlements have often expanded over areas threatened by dormant landslides [7]. The village of San Marco dei Cavoti (Benevento, Campania) is one of such southern Italy settlements affected by slope deformations causing damage to buildings and the road network. It is located on the top of a hill, at an altitude of around 700 m a.s.l. The primary outcropping lithologies are the Red Flysch and the Numidic Flysch, two structurally complex formations [8]. The main slope processes in the area are flow-like landslides, often dormant, with a complex style: as such, they trigger rotational/translational slides and then evolve into earth flows (following the terminology from Hungr et al. [9]).

Several advantages are associated with the existing methods used for landslide monitoring. Field-based monitoring techniques, such as inclinometers and extensometers, offer

direct measurements of slope deformation, providing valuable insights into the behavior of specific areas within a landslide [10–12]. Remote sensing approaches, including optical and radar satellite imagery, can cost-effectively cover vast areas, allowing for regional-scale landslide assessment and detection of changes over time [13]. Numerical modeling, encompassing limit equilibrium and finite element models, can help researchers better understand the underlying processes governing slope behavior and predict potential future movements or failure scenarios [14,15]. DInSAR analysis, as employed in this study, combines high-precision detection and monitoring of surface deformations with the ability to cover large areas, making it an increasingly valuable tool for identifying and tracking landslide activity [16,17]. Furthermore, DInSAR can be used to obtain data from areas that are difficult to access or too dangerous for field-based monitoring, increasing the safety of landslide studies [18].

Despite their advantages, the existing methods for landslide monitoring also have certain limitations. Field-based monitoring techniques, such as inclinometers and extensometers, are limited in spatial coverage, and their installation and maintenance can be expensive and time-consuming. Remote sensing approaches, such as optical satellite imagery, can be affected by factors such as cloud cover, atmospheric conditions, and vegetation cover, which may hinder the accurate detection and monitoring of landslides [19]. In the case of radar satellite imagery, such as those used in DInSAR analysis, atmospheric disturbances and the need for stable ground control points may pose challenges. Numerical modeling techniques rely on the quality of input data and the assumptions made during the model setup, which could potentially impact the accuracy of their predictions [20]. It is essential to carefully consider each method's specific advantages and limitations when selecting the most appropriate technique for landslide monitoring and assessment.

In this study, the village of San Marco dei Cavoti [21] and its immediate vicinity have been the object of a Differential Interferometry SAR (DInSAR) analysis, a powerful remote sensing technique that allows high-precision detection and monitoring of surface deformations that is being used in different fields: subsidence or uplift [22–24], sinkholes [25,26], slope processes [16,17], and monitoring of buildings [27–29]. The main products of this type of analysis are maps of mean displacement rates that show the rate at which the specific Radar Targets (RTs) move. In addition, the entire considered time series, showing the cumulative displacement for every single RT, are obtained and shown in charts for more straightforward interpretation. Thanks to its morphology and moderate urbanization, providing many surfaces that generate RTs, we obtained a great density of RTs in the area of San Marco dei Cavoti. In the context of this study, the COSMO-SkyMed mission plays a pivotal role by providing the necessary SAR data for DInSAR analysis to monitor and assess surface deformations with great detail and accuracy. Additionally, an analysis based on the decomposition of the data obtained along the Line of Sight (LoS) in two components (horizontal and vertical) has been performed using methods already presented in the literature [30], which have shown good performance in the past [31–33]. Combining the results of these analyses made it possible to obtain valuable insights into the observed deformations, thus contributing to identifying areas that may require further investigation or intervention measures.

2. Case Study

San Marco dei Cavoti is a village located in the province of Benevento, in the north-eastern part of the Campania Region (Italy). It has an extension of approximately 0.56 km² and is located at 695 m a.s.l. The area is mainly characterized by east-verging mega folds associated with reverse faults within overlapping overthrusts of different extensions, with a collective Adriatic direction. Such structures expose the clayey deposits of the Fortore Varicolored Clay Formation and the calcareous marly deposits of the Corleto Perticara Formation at the core of the folds [34,35]. The study area is mainly constituted by structurally complex formations [8] (Figure 1):

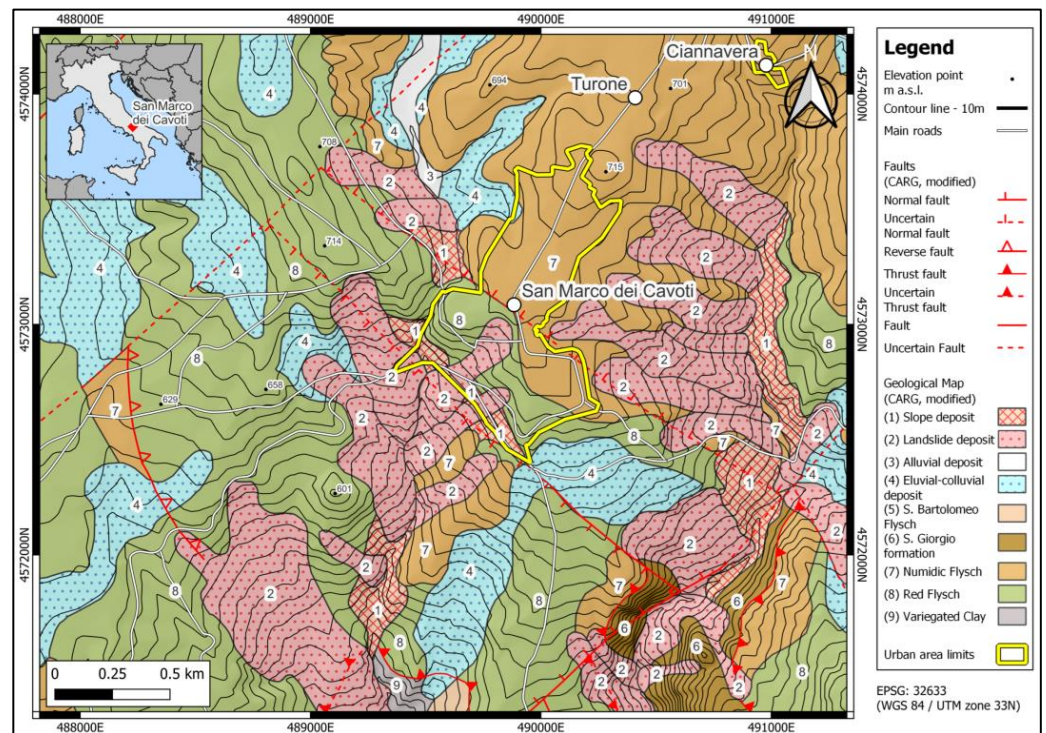


Figure 1. Geological Map of the San Marco dei Cavoti area, modified from CARG (CARTografia Geologica—Geological Cartography, the Italian project for the production of a geological map of the entire peninsula) [36]. (1) Slope deposit: sands and silts with pebbles in a silty matrix located at the base of reliefs; (2) Landslide deposits: clayey and marly deposits with lithoid fragments of calcarenites and sandstones; (3) Polygenic sands and gravels with silty-sandy matrix and levels of silty sands and clayey silts of riverbed deposits and active streams; (4) Eluvial-colluvial deposits: clayey silts with pebbles and sometimes reworked pumices and pyroclastites; (5) Alternation of sandstones with turbidite structures, clays and marly clays belonging to submarine fans (Tortonian—Messinian); (6) Sandstone-calcareous-pelitic successions (Upper Burdigalian–Tortonian); (7) Numidic Flysch (Upper Burdigalian–Upper Langhian): quartzarenites in layers and beds with thin intercalations of silty and marly clays at the base; (8) Red Flysch (Upper Cretaceous–Lower Miocene): graded calcarenites, calcilutites and crystalline limestones and interlayers of clayey marls and argillites; (9) Polychrome clays and flaky marly clays with interbedded marls, marly limestones, calcilutites, calcarenites, calcirudites and olistolites (Upper Cretaceous–Lower Miocene).

The area's geomorphology is characterized by sub-horizontal or low-slope areas in correspondence with the more erodible materials such as the argillites of the Red Flysch (Figure 2d), with values less than 15%. On the other hand, when more resistant material such as the calcirudites of the Red Flysch emerges (Figure 2e), the slopes are steeper, forming even sub-vertical walls. The hydrographic network is characterized by high drainage density in sub-basins where clayey soils outcrop with a marked evolutionary dynamic, represented by local incisions of the few alluvial covers, and some areas are affected by significant landslides [8]. The village of San Marco dei Cavoti, too, belongs to an area where slope deformations are particularly evident. The landslides within the study area affect shallow deposits, causing significant damage to structures and infrastructures (Figure 2b,c). The Southern Apennines hydrographic district reports 167 landslides that affect the entire municipality of San Marco dei Cavoti (Figure 2a).

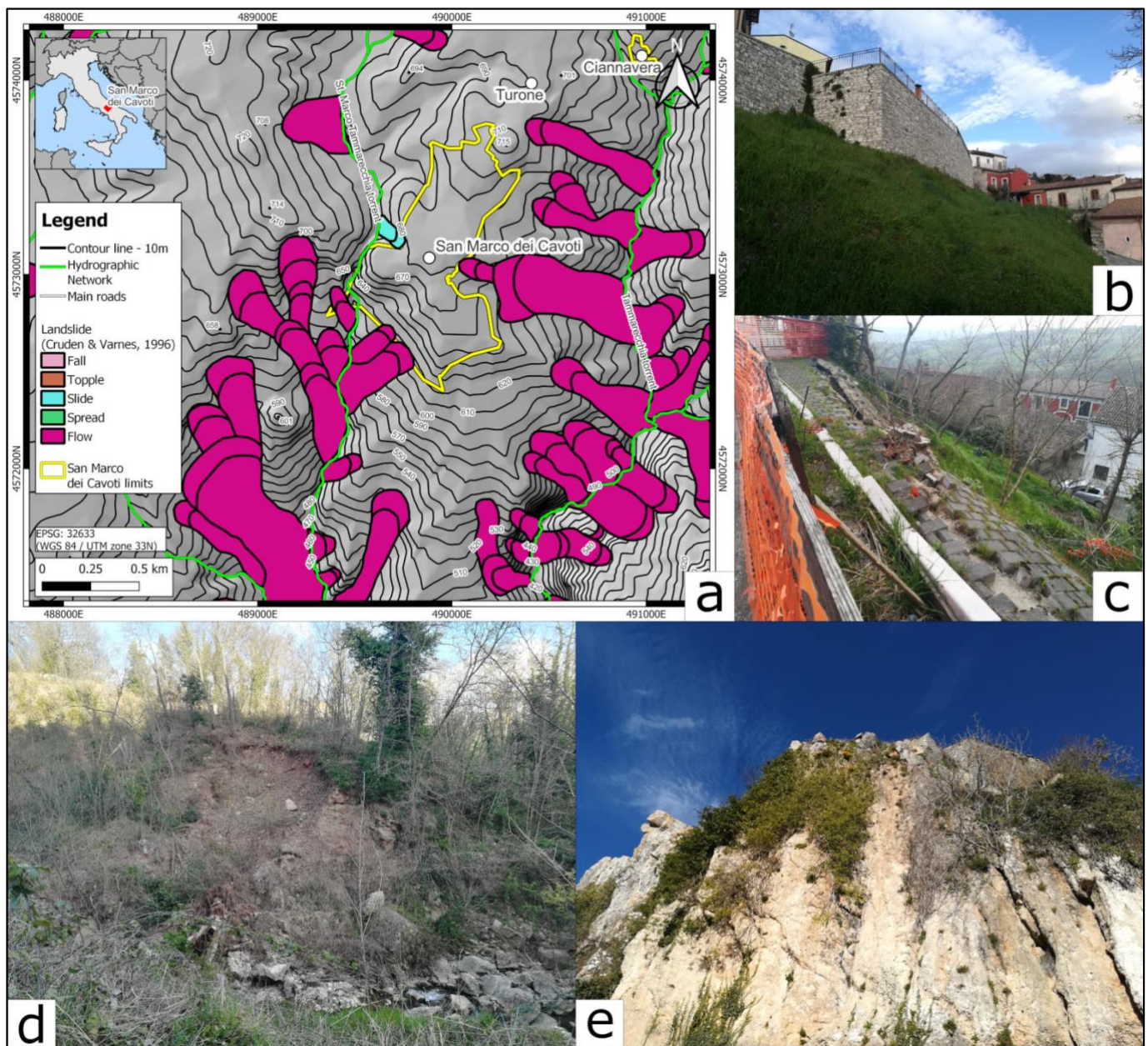


Figure 2. (a) Outline of the landslides reported by the Southern Apennines hydrographic district: detail of the area of San Marco dei Cavoti; (b,c): damage caused by the landslides to parts of the village; (d,e) argillites and calcirudites of the Red Flysch formation. These landslides differ from the data shown in Figure 1 due to the different sources and scope of the work. The first one is part of the Italian Geological Map obtained from field survey and interpretation, and the second is a landslide inventory produced for landslide study and mitigation by a different regional authority.

The Southern Apennines hydrographic district has produced the landslide inventory used in this work. These districts are the Competent Authority that manages the exploitation and protection of natural waters (surface and groundwater) and the prevention and mitigation of geohazards such as landslides, regardless of regional-administrative borders. There are seven river basin districts in Italy: Fiume Po (Po River), Alpi Orientali (Eastern Alps), Appennino Settentrionale (Northern Apennines), Appennino Centrale (Central Apennines), Appennino Meridionale (Southern Apennines), Sardegna (Sardinia), and Sicilia (Sicily).

The landslides affect flysch slopes and mainly consist of slow flows (66), rotational and translational slides (54), rapid flows (21), slides evolving to flows (18), and Deep Seated Gravitational Slope Deformation (DSGSD) (7). An area with widespread shallow landslides [4] can be recognized, too. Near the village of San Marco dei Cavoti, landslides have mainly flow-type kinematics. These landslides, which mainly affect the Red Flysch, are a significant danger to the urban fabric (Figure 2d,e), except for a slide in the Western part of the village. Other landslides are of a smaller extent and are not mapped in the landslide inventory but can be recognized during field surveys (Figure 2d,e). As far as depths are concerned, unfortunately, none of these landslides has ever been investigated with field instruments (such as inclinometers) capable of detecting the depths of the sliding surfaces.

3. SAR Datasets and Methodology

3.1. SAR Dataset

The radar images analyzed were acquired during the Map Italy Project [37], developed by the Italian Spatial Agency (ASI) and the Department of Civil Protection. The project aims to create an interferometric mapping of the entire Italian territory. It uses the StripMap HIMAGE mode (HH polarization) of the COSMO-SkyMed constellation in both Ascending and Descending modes, and it is characterized by a high image resolution (3×3 m). HH polarization further improves the quality of the collected data, providing excellent detailing of surface deformations. This satellite system is specifically designed for Earth observation and is equipped with cutting-edge sensors that operate in the X-band frequency.

Using both geometries provides a comprehensive view of the kinematics of the gravitational deformations in the study area [38]. Preliminarily, available archive image tracks were identified (Figure 3) in the area of interest, in ascending and descending geometry, characterized by the same acquisition incidence angle, a necessary condition for proper processing. Analyzing these datasets allows researchers to account for potential biases or discrepancies in the image acquisition geometry. This approach ensures that the study's results are more reliable and robust, as potential errors or inconsistencies can be identified and addressed by comparing the two datasets. Additionally, using two separate datasets, combined with an in situ survey, ensures that the study provides a comprehensive and accurate analysis of surface deformations in the area under investigation [39,40].



Figure 3. Tracks of SAR images used in the area of interest (indicated in the black square) available in the ASI archive: ascending mode (left), descending mode (right).

In detail, the image datasets processed in this study are:

- Ninety-seven images were acquired in ascending geometry from 6 January 2017 to 12 November 2022.
- Eighty-one images were acquired in descending geometry from 28 January 2017 to 29 October 2022.

Specifically, the images recorded in ascending orbit have an incidence angle of 29.2° , while those acquired in descending orbit have an inclination of 31.9° relative to the vertical.

3.2. Coherent Pixels Technique

The algorithm used for processing satellite radar images is the “Coherent Pixels Technique” (CPT), developed by Mora et al. [41] and then implemented by Iglesias et al. [42] with Temporal Phase Coherence (TPC) at the Remote Sensing Laboratory (RSLab) of the Universitat Politècnica de Catalunya (UPC). This algorithm allows the development of the entire interferometric chain using image pairs with reduced spatial and temporal baselines, thus characterized by a better phase response. The CPT-TPC is a robust algorithm that effectively processes satellite radar images to show surface deformations. Its unique capability to work with image pairs characterized by reduced spatial and temporal baselines results in a better phase response, which is crucial for obtaining accurate information about such deformations. Additionally, CPT-TPC is known for its robustness against atmospheric disturbances and decorrelation noise, making it a reliable choice for this study. One of the strengths of CPT-TPC is its ability to select radar targets (RTs) that exhibit good electromagnetic response stability. RTs are reflectors materializing as existing ground elements, such as manufactured structures (buildings, monuments, roads, railways, pylons) or natural elements (rock outcrops). Therefore, they generally cannot be found in areas characterized by widespread vegetation. Analogous to geodetic networks, the set of RTs identified in an area under investigation can be considered a dense natural network of measurement points whose positions and movement velocities are referred to as fixed points, assumed as stable over time, having recorded determined coherence values. During processing, the velocity of these reference points is conventionally set equal to zero. By focusing on these stable reflectors, the algorithm reduces the impact of errors and noise in the final output, thus enhancing the results’ accuracy.

The processing procedure consists of three main phases:

1. Generation of the best interferograms from the available image dataset.
2. The selection of RTs characterized by a fixed phase value is considered indicative of good electromagnetic response stability;
3. Calculate average displacement velocities and the temporal displacement series of the selected points in the considered observation period.

The output results obtained from CPT-TPC processing are generally characterized by a high degree of precision and accuracy intrinsic to the algorithm.

The precision of the measurements indicates the degree of convergence of the measured values around their mean, while accuracy quantifies the distance between the measurements and the actual data. Regarding interferometric data, issues related to precision and accuracy involve the georeferencing of reflectors, the determination of the mean displacement rate, and the determination of the time series of displacement. Concerning the spatial positioning of reflectors, the conversion from SAR coordinates to UTM-WGS84 (here Z33N) coordinates is affected by a positioning error in the North–South and East–West directions, equal to ± 5 m. The presence of disturbances, such as atmospheric and decorrelation noise, results in error in the velocity measurement of the order of ± 5 mm/year. The error related to the ellipsoidal height of each point is estimated at ± 1.5 m.

3.3. Vertical and Horizontal Component Analysis

SAR satellites follow specific semi-polar (North–South) orbits and acquire information in the West–East direction (Figure 4) [38]. This means that, for ascending data, positive values move toward the satellite in the East–West direction, while negative data moves away from the satellite in the West–East direction. On the other hand, the positive descending data moves toward the satellite in a West–East direction, and the negative data in an East–West direction. It is possible to obtain the displacement components in the West–East and vertical directions by knowing the direct cosines of image acquisition, as shown in Figure 5. In this work, a MATLAB script [43] was implemented to decompose the movement. The first step requires the production of a grid (the MATLAB script allows one to choose the grid dimension).

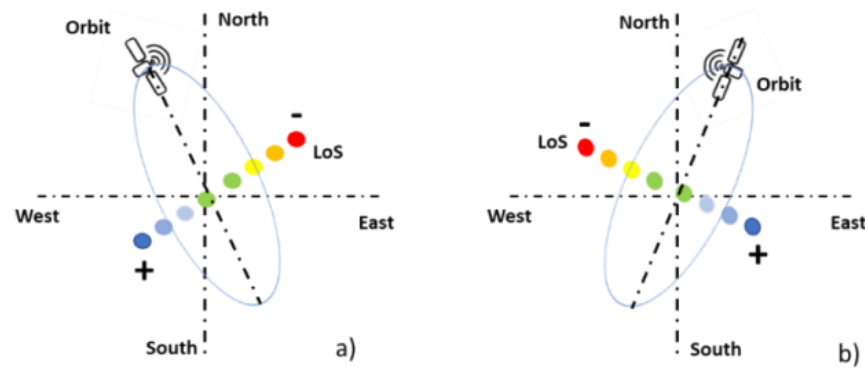


Figure 4. The geometry of acquisition: (a) ascending, (b) descending. The warm color palette indicates the direction of movement away from the satellite (-) while the cold color palette indicates the direction of movement towards the satellite (+).

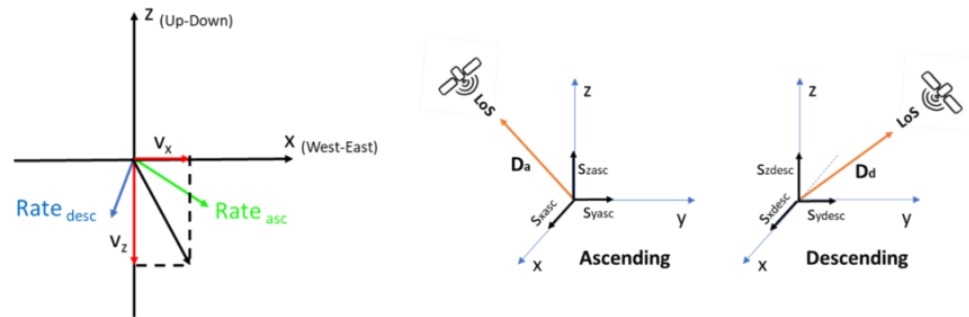


Figure 5. Geometric representation of the decomposing of the data.

After the first step, the script calculates the number of ascending and descending RTs located within each cell and their mean rate value. Once this grid has been produced, three different formulas are applied, depending on the amount of ascending and descending RTs in the cell.

In case there are both ascending and descending RTs inside of a cell, the formula [30] used is:

$$v_z \text{ (Vertical Component)} = \frac{(Rate_{desc} \times Sx_{asc}) - (Rate_{asc} \times Sx_{desc})}{(Sx_{asc} \times Sz_{desc}) - (Sx_{desc} \times Sz_{asc})} \tag{1}$$

$$v_x \text{ (Horizontal Component)} = \frac{(Rate_{asc} - v_z \times Sz_{asc})}{Sx_{asc}} \tag{2}$$

where:

- $Rate_{asc}$ and $Rate_{desc}$ are the velocities obtained from the ascending and descending data;
- Sx_{asc} is equal to $-\sin(\vartheta_{asc}) \times \cosin(\tau_{asc})$;
- Sz_{asc} is $\cosin(\vartheta_{asc})$;
- Sx_{desc} is equal to $-\sin(\vartheta_{desc}) \times \cosin(\tau_{desc})$;
- Sz_{desc} is $\cosin(\vartheta_{desc})$;
- τ is the angle between the orbit of the satellite and the North (heading angle);
- ϑ is the incident angle.

If inside of the cell there are ascending RTs and no descending RTs, the formula used is:

$$v_{zasc} = \frac{Rate_{asc}}{\cosin(\vartheta_{asc})} \tag{3}$$

$$v_{xasc} = -\frac{Rate_{asc}}{\sin(\vartheta_{asc})} \tag{4}$$

On the other hand, when there are only descending RTs, the formula does not change:

$$v_{zdesc} = \frac{Rate_{desc}}{\cos(\vartheta_{desc})} \quad (5)$$

$$v_{xdesc} = \frac{Rate_{desc}}{\sin(\vartheta_{desc})} \quad (6)$$

From these formulas, we obtained the values related to the satellite “reference” system (positive when it moves toward the satellite, negative when it moves away from it). As shown in Figure 5, to obtain a value suitable for our cartesian coordinate system, we have to multiply the value obtained in V_{xasc} with -1 . That is because it is customary to have the positive side of the x -axis going toward the first and fourth quadrants. Instead, the values obtained from the ascending data are negative when they move toward the East. As for the vertical components, there is no need to intervene on the formulas because, in both cases, the movement towards the satellites corresponds to moving along the z -axis towards its positive values.

4. Results and Discussion

In the Results and Discussion section, we present and analyze the data obtained from the DInSAR technique employed to monitor surface deformations in the area of San Marco dei Cavoti. The study focuses on ascending geometry from 6 January 2017 to 12 November 2022 and descending geometry from 28 January 2017 to 29 October 2022. The components obtained from interferometry are also analyzed to characterize the detected slope movements. The section will start with an overview of the data processing and analysis methods, followed by a detailed discussion of the observed deformation patterns.

4.1. Ascending Dataset Results

The image processing was conducted using the CPT-TPC algorithm, which analyzes RTs directly identified on the ground, allowing the evaluation of any displacement over time.

The first step of the processing was the co-registration. The master image was automatically identified by the software, which is capable of selecting it, minimizing total decorrelation in generating all interferograms. As discussed earlier, 97 images acquired in ascending geometry from 6 January 2017 to 12 November 2022 were used, and 352 interferograms were generated (Figure 6), allowing the analysis of individual pixels that show a specific quality/stability in terms of phase.

Specifically, the acquisition on 8 August 2019 was chosen as the master image for the co-registration of the entire stack of images. After that, the first results obtained from the elaboration are (Figure 7): (a) the Radar Targets Map and (b) the Triangulation Map.

In particular, the Radar Targets identified map (Figure 7a) shows the points on the ground that generates a consistent radar signal over time. By analyzing the displacement of these Radar Targets, we can obtain accurate information on surface deformations in the study area. The Radar Targets identified image provides a visual representation of the distribution of these targets and their displacement patterns, aiding our interpretation of the landslide dynamics. On the other hand, the Triangulation Map images (Figure 7b) are used to display the interferometric phase measurements for each Radar Target, which are then converted into displacement values. These images help us understand the spatial distribution of the measured displacements and identify areas with significant deformation. By comparing the Triangulation Map images obtained from ascending and descending geometries, we can also gain insights into the different displacement components, such as vertical and horizontal movements. At the end of the processing, both the mean displacement rate map along the LoS of the RTs (Figure 8) and the time series were provided. It should be emphasized that the latter represents cumulative displacements from the first available image, while the mean displacement rates represent a sort of linear velocity that

the model estimates over the entire acquisition interval. As can be seen, a high number of RTs (about 53,188) were identified in the investigated area, resulting from the outstanding electromagnetic response of existing structures. In contrast, heavily vegetated environments are characterized by fewer targets, making them difficult to investigate. In detail, 27,504 RTs were used in ascending geometry to analyze the San Marco dei Cavoti village, with a density of approximately 7457 RT/km². These targets present mean displacement rates along the LoS up to 2.5 cm/year, particularly in the western sector of the study area. Overall, the recorded displacement rates refer to slow kinematics, with maximum displacement velocities of a few centimeters per year. As shown in Figure 8, the most interesting area is located close to the San Marco dei Cavoti village, to the southwest. The area shows several substantial amount RTs with high rates.

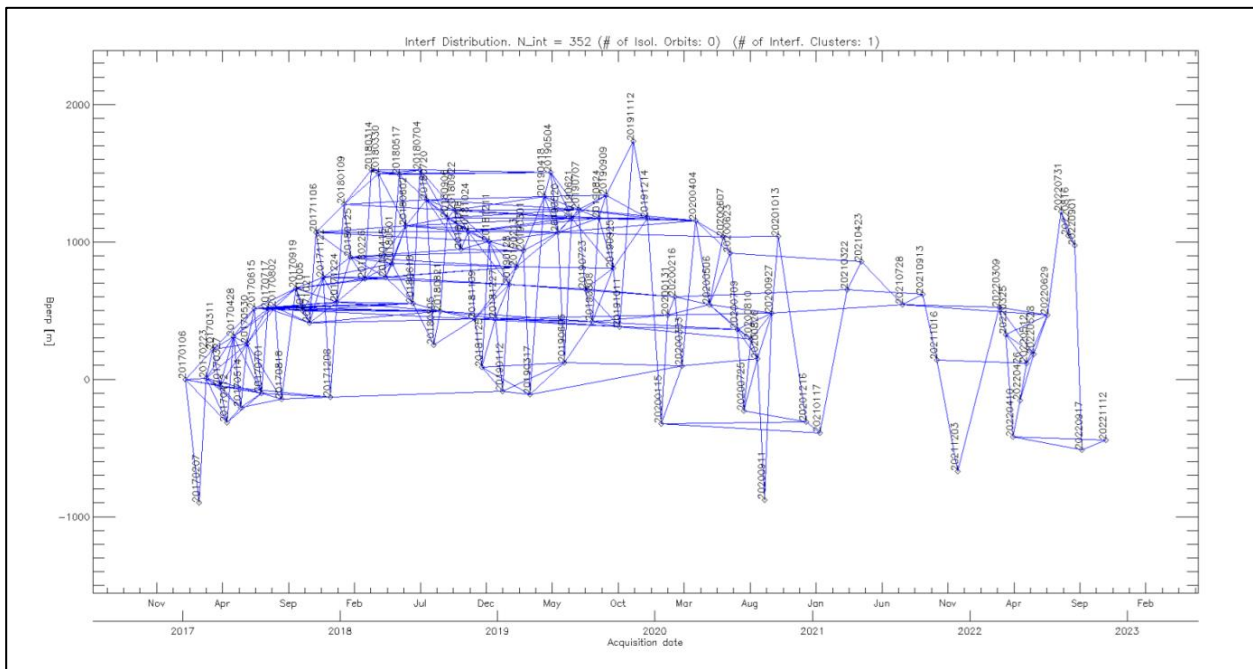


Figure 6. Interferogram distribution in ascending geometry in the analyzed time interval.

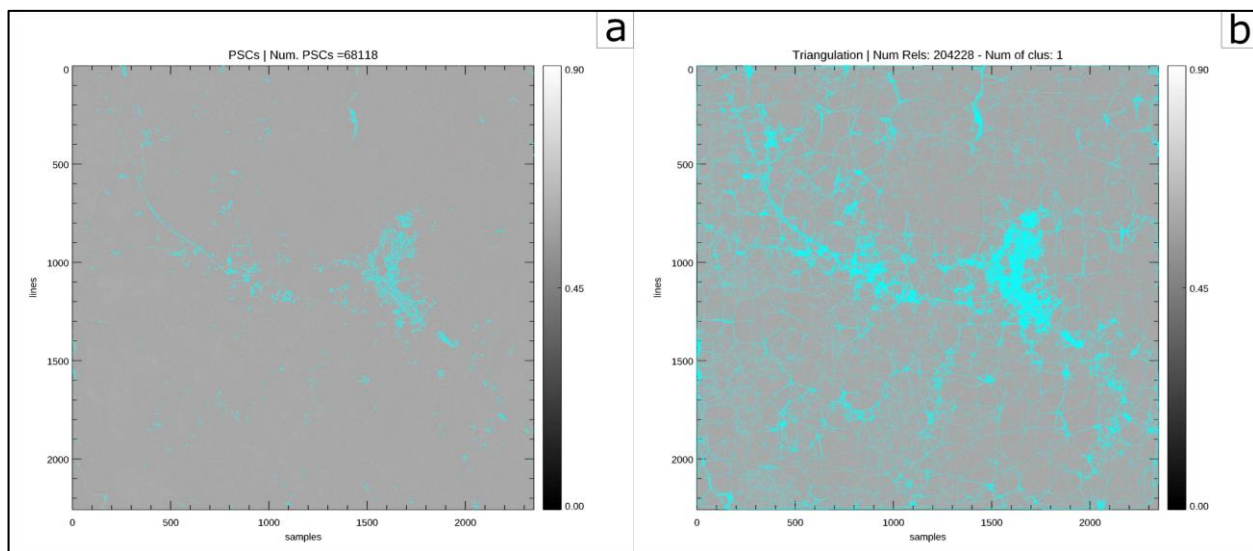


Figure 7. (a) Radar Targets identified; (b) Triangulation Map.

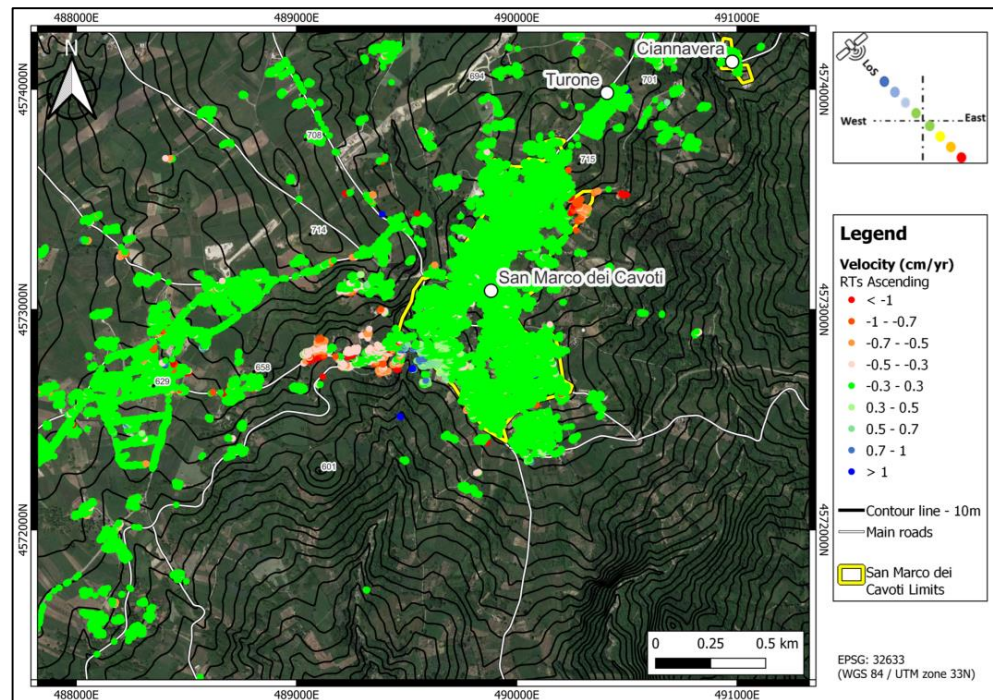


Figure 8. Map of the average displacement rate along the “LoS” of the targets identified in ascending geometry.

4.2. Descending Dataset Results

Similar to the discussion in the previous section, 81 images acquired in descending geometry were processed from 28 January 2017 to 29 October 2022 (Figure 9) using the CPT-TPC algorithm. This approach allows the analysis of 240 interferograms defined from the available image dataset, enabling an analysis of individual pixels that show a specific quality/stability in terms of phase. The software selected as the master acquisition for the entire stack, the one obtained on 25 August 2019.

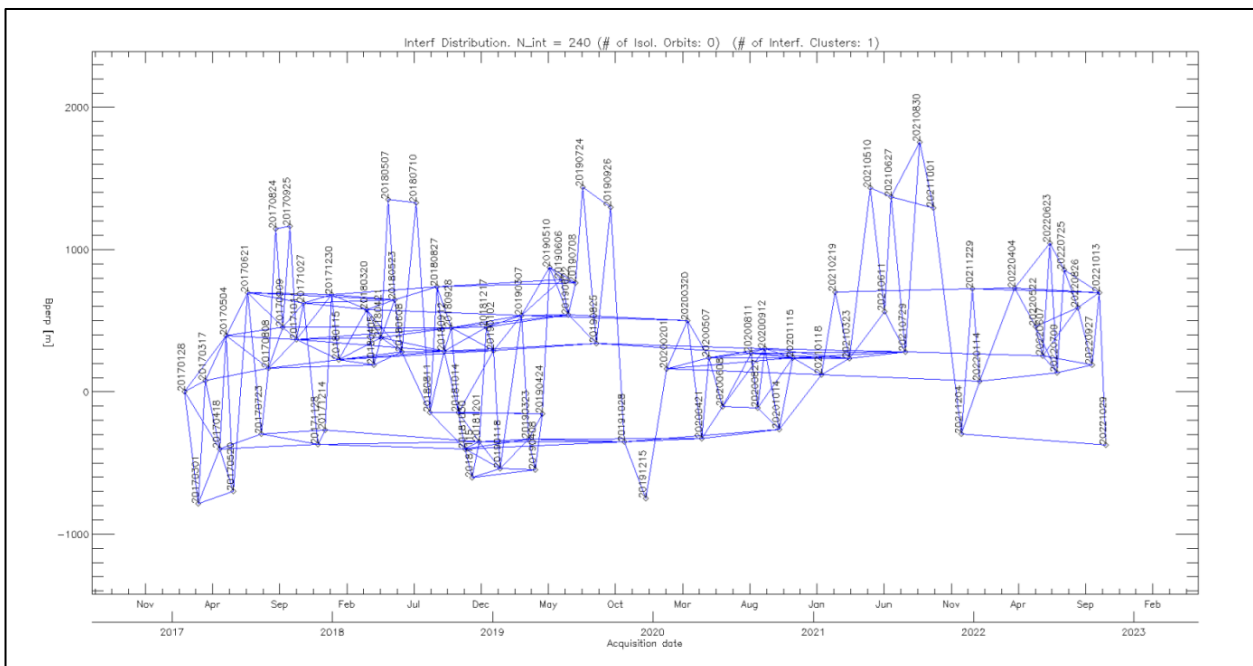


Figure 9. Interferogram distribution in descending geometry in the analyzed interval.

Just as before, the Radar Targets Map (Figure 10a) and the Triangulation Map (Figure 10b) were produced for the ascending geometry.

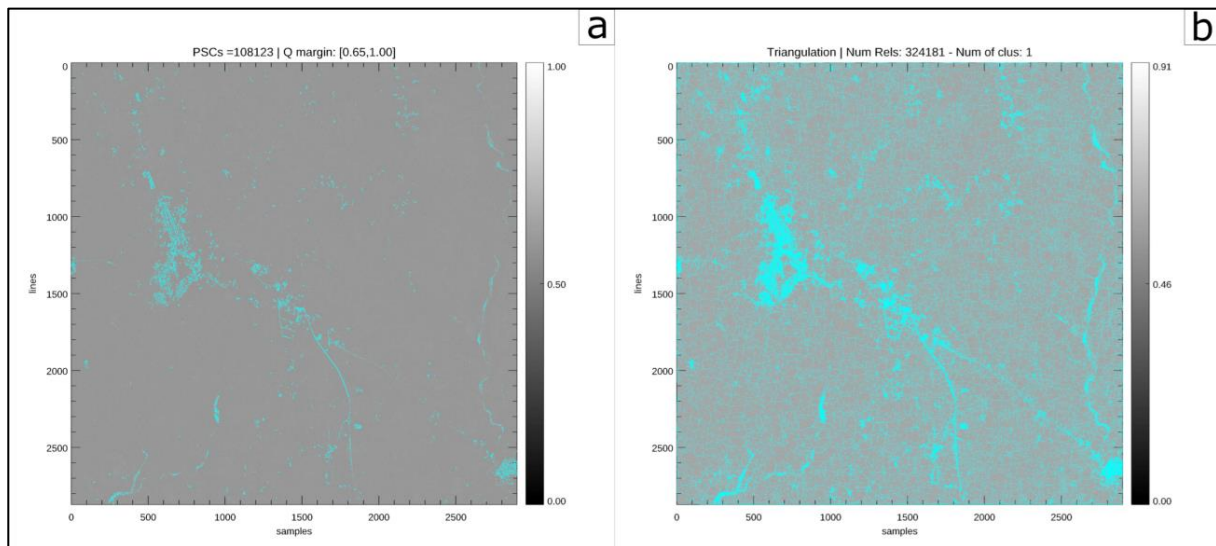


Figure 10. (a) Radar Targets identified; (b) Triangulation Map.

It should be noted that the latter represents cumulative displacements from the first available image, while the average velocities represent a linear speed that the model estimates over the entire acquisition interval. As can be seen (Figure 11), a target density of the same order of magnitude as that obtained in ascending geometry (about 59,132 RTs) was obtained: a high number of reflectors is identified in correspondence with the existing infrastructure and urbanized network, depending on the electromagnetic response of the existing artifacts; again, heavily vegetated environments are characterized by a reduced number of targets, making them difficult to investigate.

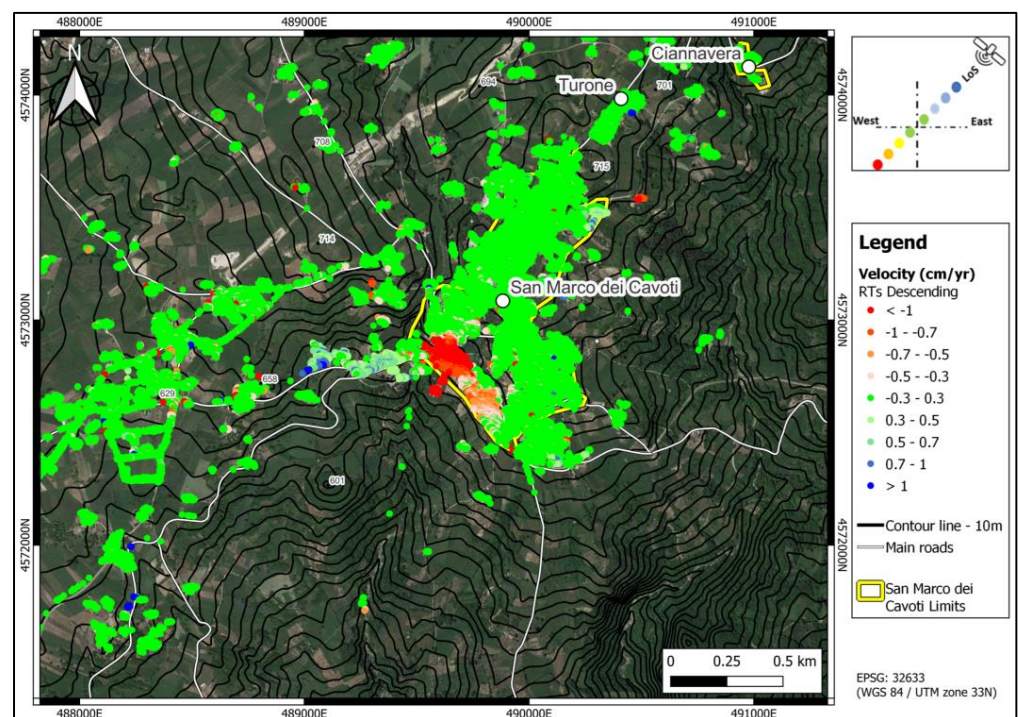


Figure 11. Map of the average displacement rate along the “LoS” of the targets identified in descending geometry.

In detail, the analysis of the infrastructure's surrounding area revealed 29,484 targets in descending geometry, with a density of approximately 7994 RT/km². These targets exhibit average displacement velocities along the LoS up to approximately 30 mm/year maximum. This maximum displacement was recorded in the western sector of the study area. The displacement rates observed in descending geometry, as previously discussed for ascending acquisitions, confirm the occurrence of very slow kinematics. This slow movement can be attributed to a combination of factors, including the regional tectonic setting, local geological and geomorphological conditions, and anthropogenic influences such as groundwater extraction and urban development. In the urban area of San Marco dei Cavoti, a non-negligible displacement zone can also be detected in the descending geometry. These displacements along the LoS can reach a rate of up to 20 mm/year. This area of increased displacement could be associated with local geological conditions or anthropogenic factors, such as building construction or land use changes.

The results obtained from both ascending and descending acquisitions provide a more comprehensive understanding of the ongoing deformation processes in the study area. These insights can inform land-use planning, infrastructure maintenance, and disaster risk reduction strategies, ensuring the long-term safety and sustainability of the area. Further investigation may be required to determine the exact cause of this observed movement and assess potential threats to the local community.

4.3. San Marco dei Cavoti Village: Time Series and Analysis of Vertical and Horizontal Components with MATLAB

The time series of six ascending (Figure 12) and six descending (Figure 13) RTs have been produced. These RTs have been chosen by considering both the presence of already inventoried landslides and by searching for the more interesting high-rate related areas. The location of these twelve points is shown in the following figures.

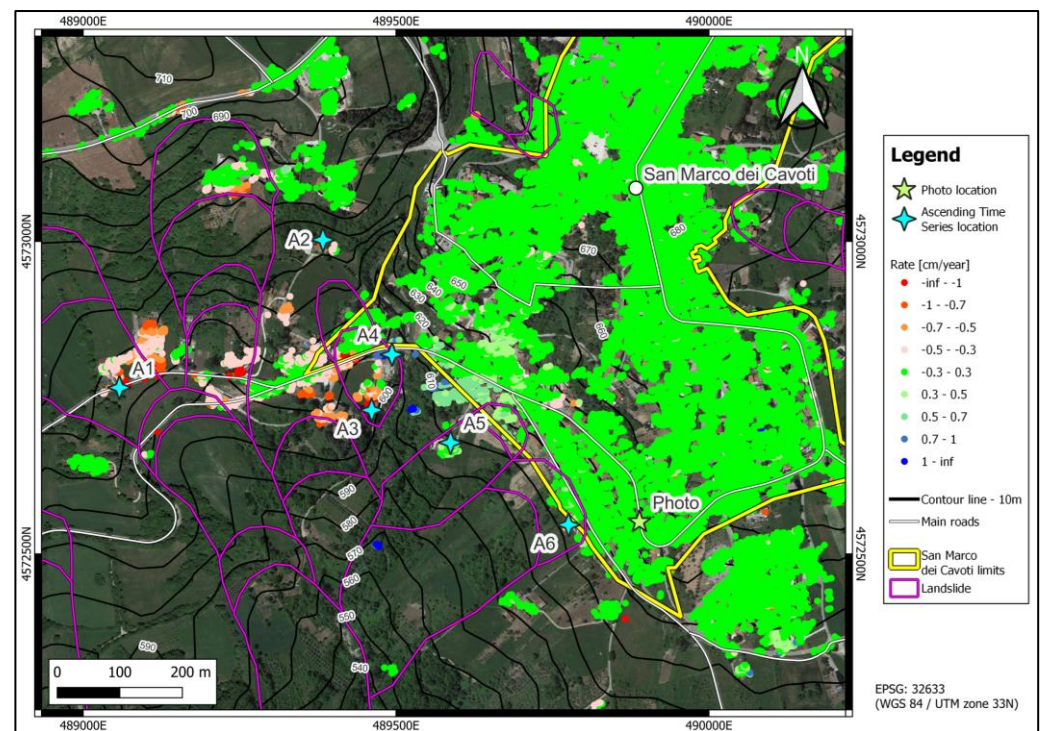


Figure 12. Location of ascending time series (A1–A6).

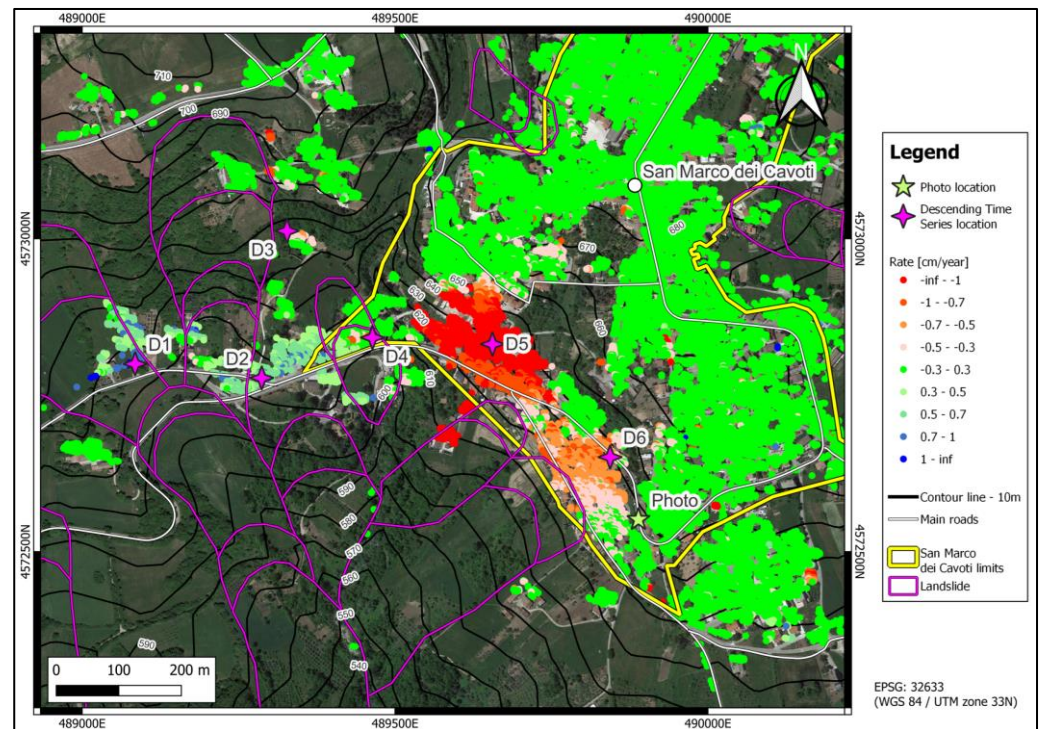


Figure 13. Location of descending time series (D1–D6).

As shown in the graphics (Figure 14), the ascending time series located on top of already recognized landslides (A1 and A3–A6) show the presence of a trend. This is interpreted as the landslide is still active, although moving slowly. The A2 time series is interesting as it shows a certain displacement (up to -6 mm) in a zone where no landslide was previously recognized. This could be a sign of the presence of a slope process that could have either (i) not been recognized because of the vegetation or human activities and (ii) an uphill, retrogressive enlargement of the already recognized landslide. Something similar happens with the descending time series: D1 and D4, located on a landslide, show slow movements, most likely related to the landslide.

On the other hand, D2, D3, D5, and D6 are located on the slope in zones where there are no recognized landslides. Especially in the case of D5 (up to 14 mm of displacement), these movements are most likely related to landslide activity. D5 and D6 are located uphill of landslides in the San Marco dei Cavoti village's limits.

A similar result is obtained from the analysis made with the decomposition of the rates. Combining the Ascending and Descending data, it is possible to decompose the velocity obtained along the LoS of the satellites. It should be noted that only the horizontal (W–E direction) and the vertical decomposition analysis can be performed. This is due to the satellite orbits, which are almost perfectly N–S. Displacements along the same direction of the satellite are not detected, which means that a perfectly N–S-oriented landslide is more challenging to detect than a W–E-oriented one. Given the morphology of the area southwest of San Marco dei Cavoti (Figures 12 and 13), the satellites can detect the landslides within the area in both ascending (landslides along the slope exposed to the SW) and descending (landslides along the slope exposed to the SE) geometries. Since the remaining part of the analysis carried out is based on the kinematic relationships between the W–E components and the vertical components, the lack of the N–S component has a negligible impact on our study.

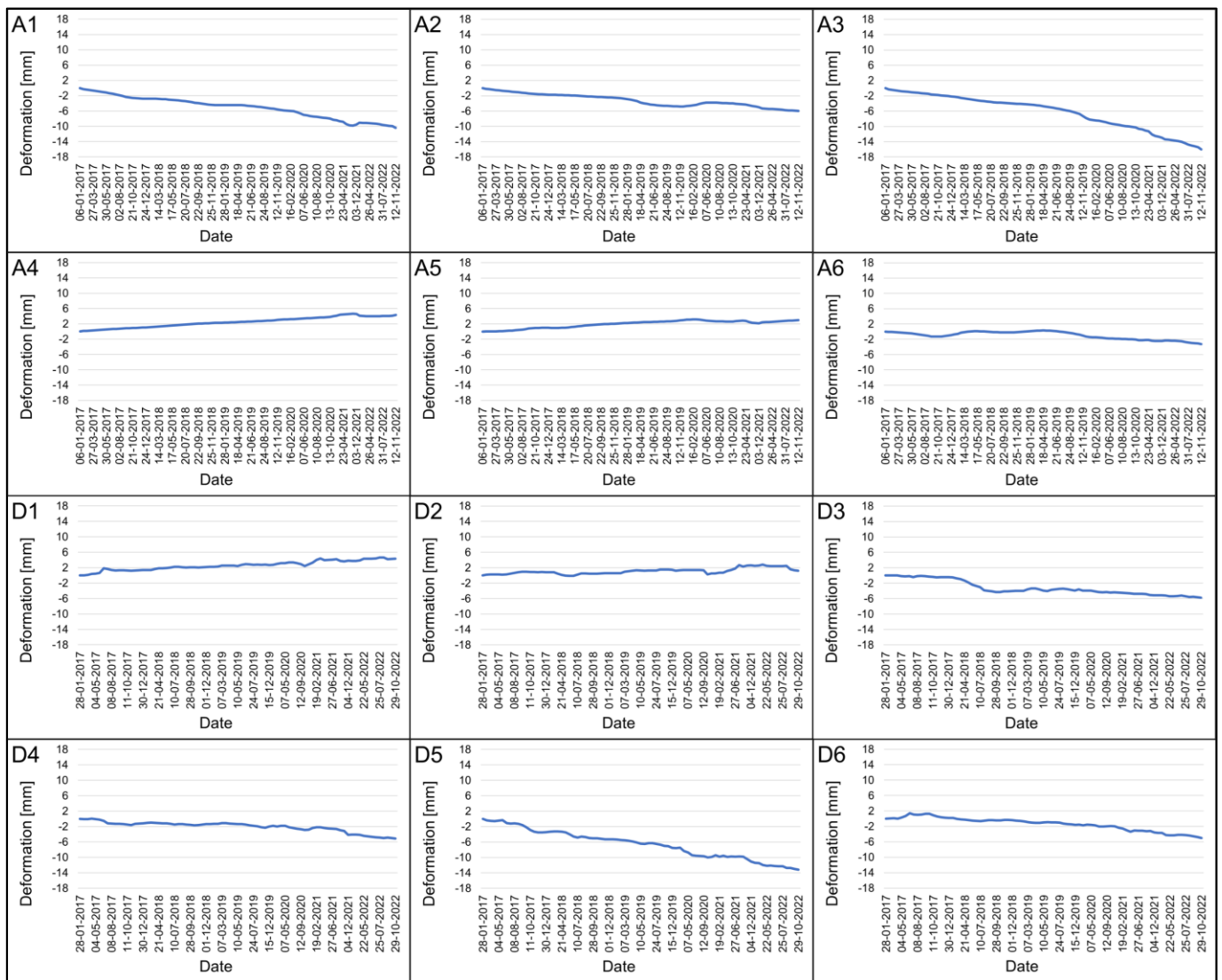


Figure 14. (A1–A6) Ascending time series. (D1–D6) Descending time series.

Usually, when the original data from the two geometries show a discordant movement (Figures 14 and 15), the predominant component is the horizontal one. On the other hand, when the ascending and descending data show a concordant movement, the main component of the rate is the vertical one. Comparing the ascending and descending geometries allows us to assess the potential failure mechanisms that might be driving the observed surface deformations. By examining the spatial distribution of vertical displacement rates, we can explore whether the data points to specific failure mechanisms, such as roto-translational or planar displacement. For instance, if the spatial distribution of vertical displacement rates reveals greater values at the rear of the unstable area, it could indicate a roto-translational mechanism.

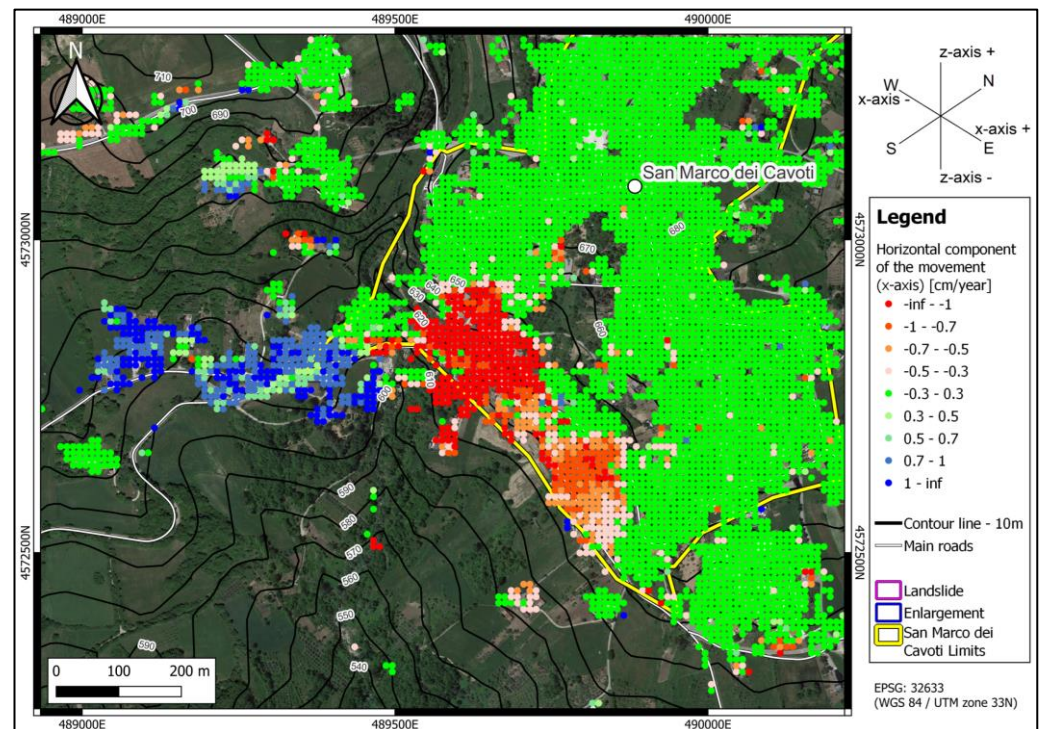


Figure 15. The horizontal component of the mean displacement rate.

On the other hand, if the rates appear to be spatially homogeneous, it might suggest a planar displacement mechanism. As the resolution of the COSMO-SkyMed data is 3 m, these components are obtained using a 10 m sized grid cell. This way, more data are usually used during the computation. The two components are the horizontal one along the x -axis (E–W) (Figure 15), which shows a maximum rate of -5.7 cm/year (towards the West) and 4.9 cm/year (towards the East), and the vertical one (along the z -axis, as the N–S direction is the y -axis) (Figure 16), showing a top rate of 1.4 cm/year (uplift) and -3.4 cm/year. The obtained movements comply with the existing data and the geomorphology, as the landslide right next to the village of San Marco dei Cavoti is located on a southwest-facing slope. This follows the observed horizontal component, which is negative (towards the West).

As shown in Figures 8 and 11, most of the movement is located along the slopes in the South and southwest areas of the village, while the rest of San Marco dei Cavoti appears to be stable. The results also show that, as the horizontal component of the velocity is the most prominent of the two, the main movement type for these landslides is translational sliding. When the vertical component is the main one, on the other hand, it usually means that the main movement type is rotational sliding, as the geometry of the detachment surface allows, sometimes, a more prominent vertical displacement than the horizontal one. Looking at the map, it also appears that some deformations had not been observed in the past (Figure 17).

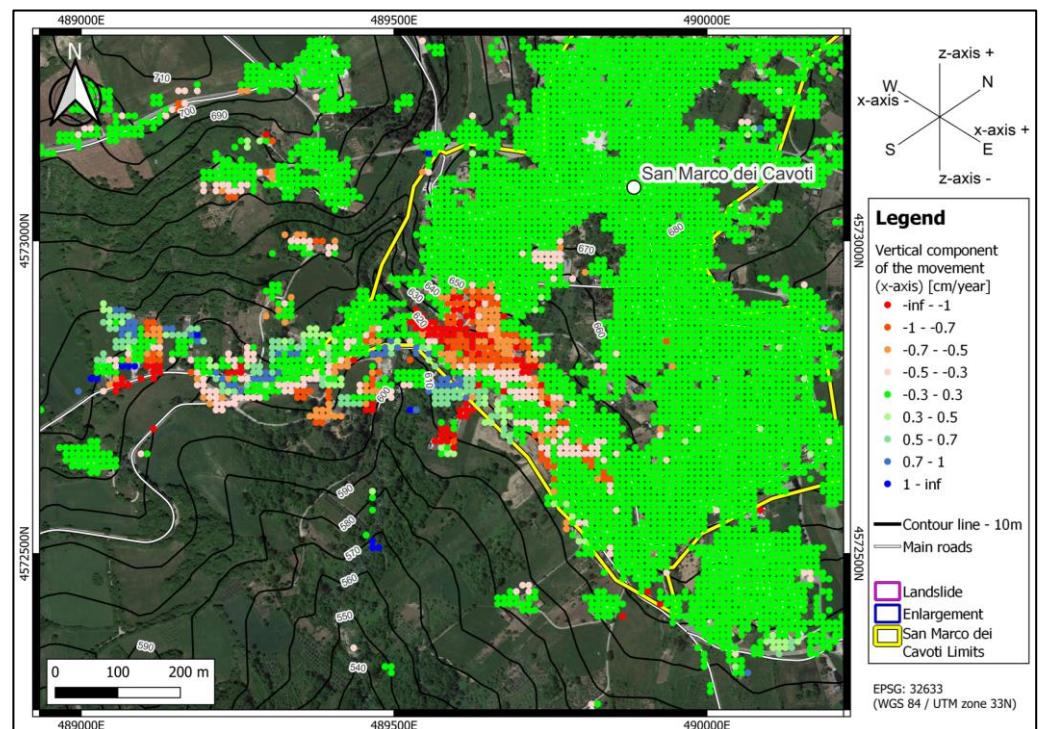


Figure 16. The vertical component of the mean displacement rate.

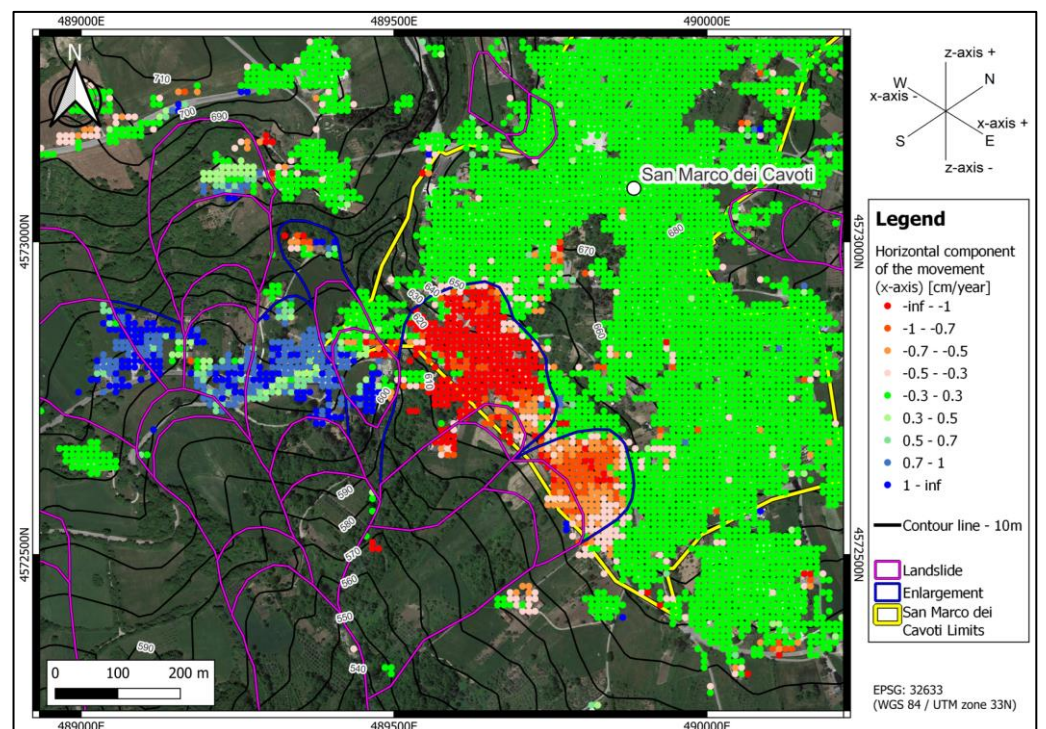


Figure 17. The horizontal component of the mean displacement rate and comparison to the Landslide inventory.

The areas characterized by anomalous movements detected by the DInSAR technology are enclosed within the blue polygons in Figure 17. These areas are not part of the used inventory, and the reasons may be related to either the effect of human activities that have covered the traces of slow movements or the satellite-based detection of new, retrogressive enlargement of the landslides. In Figure 17, the proposed areas in blue show high velocity

and could be the subject of a future landslide remapping proposal. As shown in Figure 18, one of these landslides has already affected and damaged the road infrastructure. The other two landslides near the San Marco dei Cavoti village center (N and NE portion of Figure 16) appear stable. This aligns with the information obtained from the landslide inventory, which labels those two landslides as dormant. Further analysis of the results obtained shows that:

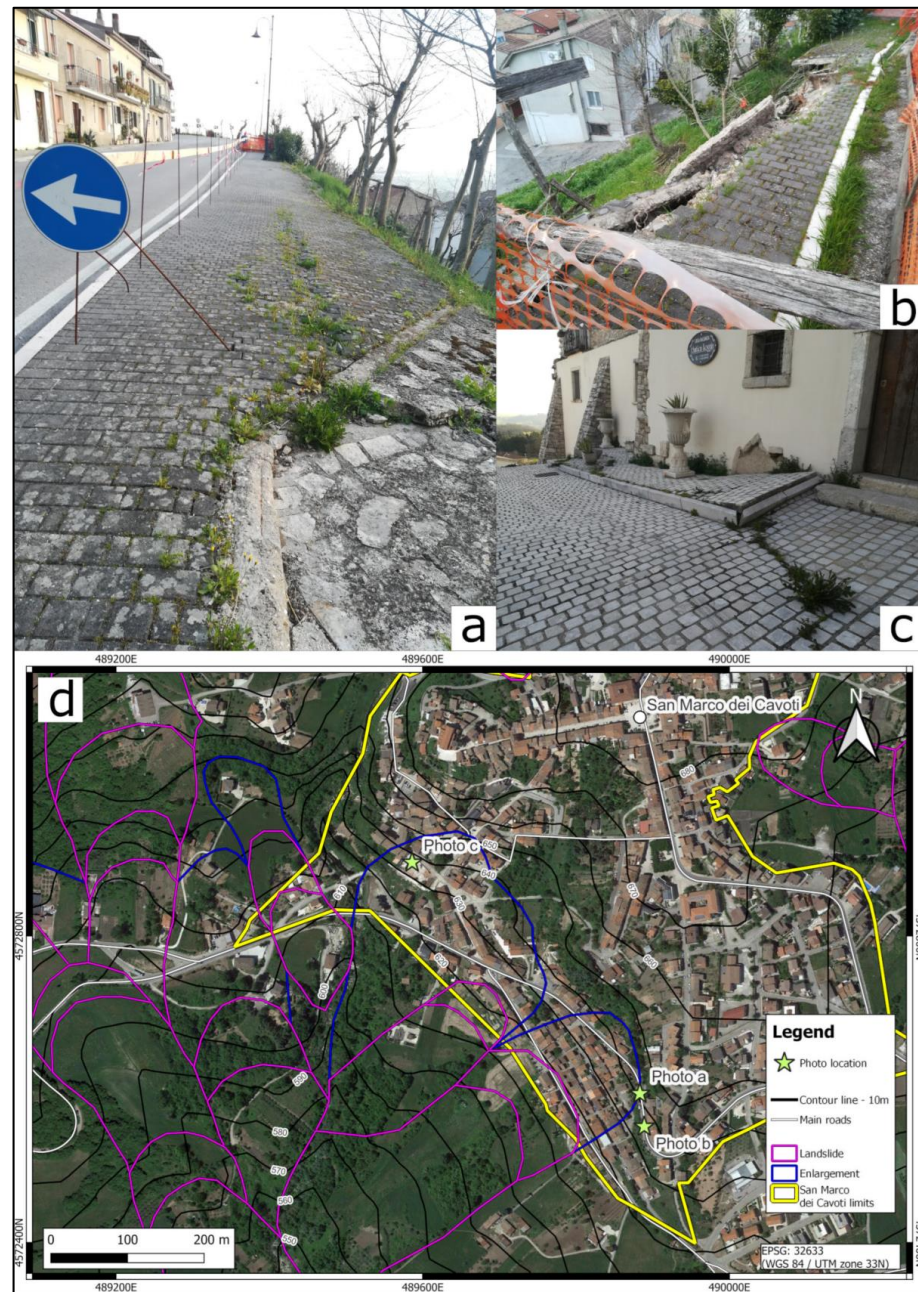


Figure 18. (a,b) Crown cracks and road damage along the Crown detected on the Ex Strada Statale 369; (c) Damage to the buildings and the plaza next to Via Mercato; (d) Position of the landslides evidenced in the photos on the map.

(1) The foot of the landslide is covered by vegetation and does not return RTs that can be analyzed. This could be resolved by using artificial corner reflectors, as already completed, with good results, for other landslides in Flysch formation in South Italy [44] where the visibility was not optimal;

(2) Along the slope, the prevailing component of the movement is the horizontal one, but in the upper part of the slope, it is possible to notice an increase in the vertical component in the enlargement area. This type of kinematics, especially the evolution in flow landslides, is quite common in Flysch formation [45], and the uphill enlargement is a phenomenon seen in other Red Flysch landslides [46].

This increment in vertical component on the upper side of the slope is probably due to either a local rotational movement of the landslide or vertical deformations due to road cuts in correspondence with the urban area of the hamlet. As seen in Figure 16, along the western border of the San Marco dei Cavoti urban area, the vertical component of the displacement rate tends to zero or even towards positive values along the slope. It is, then, highly probable that the kinematics of the slope process is indeed related to a local rotational slide.

5. Conclusions

This paper presents the interferometric results in ascending geometry (from 6 January 2017 to 12 November 2022) and descending geometry (from 28 January 2017 to 29 October 2022), related to monitoring surface deformations using the Differential SAR Interferometry technique in the area surrounding the village of San Marco dei Cavoti. The results are displayed as average displacement rate maps and displacement time series along the sensor–target LoS direction for the identified targets in both acquisition geometries and for vertical and horizontal components of the rate.

The complex morphology of the area and its moderate urbanization, along with the presence of structures and infrastructures, provide a good number of reflectors with similar density for ascending and descending geometries (respectively, 7457 and 7994 RT/km²). In heavily vegetated areas with no direct ground reflectors, the density of monitorable points significantly decreases; this issue could be resolved by installing a network of artificial corner reflectors characterized by excellent electromagnetic wave reflectivity. Regarding the village of San Marco dei Cavoti, the high density of RTs allowed identifying and confirming some sectors with more significant displacement rates, up to a few cm/year. In particular, the analysis of displacement time series for some targets identified in areas already affected by landslides confirms the slow kinematics of the deformation phenomena. The time series analysis shows that the already recognized landslides are active, often showing retrogressive processes. This conclusion is strengthened by analyzing the decomposition of the ascending and descending rates into the two horizontal (W–E axis) and vertical components.

Thanks to the data obtained from the decomposition of the rates, we obtained different information:

- Small displacements are still detected in the already mapped landslides. This could be either a reactivation of the landslides, or they never stopped their displacement with a slow velocity. As most of the slope is covered by vegetation, the toes of the landslides cannot be analyzed.
- The analysis also showed displacements uphill from the mapped landslides. These areas could be related to either an enlargement of the landslides or those could have been part of the landslide since the first activation but were not detected, as urban areas can, sometimes, make it more difficult to find evidence of slow velocity landslides. The presence of the landslide crowns is confirmed by field survey (Figure 18a–c).
- The cinematic obtained through the decomposition analysis confirms the type of movement related to the mapped landslides (mostly slides that feed shallow flow landslides). As for the displacement areas not mapped in the inventory, we can suppose the presence of a rotational type of slide, as the uphill vertical displacement is higher than the horizontal one and, along the slope, the vertical displacement becomes the lesser of the two.

As shown, such an analysis is an additional tool that can be useful for both landslide monitoring and preliminary investigation. In this case, the satellite data obtained from

the decomposition confirmed the studied slope processes and their characteristics (type of movement, velocity). Finally, further investigation could lead to estimating the depth of the sliding surfaces [47].

Author Contributions: Conceptualization, D.D.M. and M.A.K.; methodology, M.A.K., G.B. and D.D.M.; software, M.A.K. and G.B.; validation, M.A.K.; formal analysis, M.A.K., G.B. and C.D.M.; investigation, M.A.K.; resources, D.D.M.; data curation, M.A.K. and G.B.; writing—original draft preparation, M.A.K., G.B. and C.D.M.; writing—review and editing, S.P.Z.; supervision, D.D.M. All authors have read and agreed to the published version of the manuscript.

Funding: The authors received no financial support for this article’s research, authorship, and/or publication.

Data Availability Statement: Data available under motivated request.

Acknowledgments: The project was carried out using COSMO-SkyMed Products, © of the Italian Space Agency (ASI), delivered under a license to use by ASI. The authors are grateful to the anonymous reviewers for providing helpful suggestions.

Conflicts of Interest: The authors declare no conflict of interest.

References

- Guzzetti, F. Landslide Fatalities and the Evaluation of Landslide Risk in Italy. *Eng. Geol.* **2000**, *58*, 89–107. [CrossRef]
- Froude, M.J.; Petley, D.N. Global Fatal Landslide Occurrence from 2004 to 2016. *Nat. Hazards Earth Syst. Sci.* **2018**, *18*, 2161–2181. [CrossRef]
- Del Soldato, M.; Di Martire, D.; Bianchini, S.; Tomás, R.; De Vita, P.; Ramondini, M.; Casagli, N.; Calcaterra, D. Assessment of Landslide-Induced Damage to Structures: The Agnone Landslide Case Study (Southern Italy). *Bull. Eng. Geol. Environ.* **2019**, *78*, 2387–2408. [CrossRef]
- Cruden, D.M.; Varnes, D.J. Landslide Types and Processes. *Spec. Rep.-Natl. Res. Council. Transp. Res. Board* **1996**, *247*, 36–57.
- Guerriero, L.; Confuorto, P.; Calcaterra, D.; Guadagno, F.M.; Revellino, P.; Di Martire, D. PS-Driven Inventory of Town-Damaging Landslides in the Benevento, Avellino and Salerno Provinces, Southern Italy. *J. Maps* **2019**, *15*, 619–625. [CrossRef]
- Discenza, M.E.; Esposito, C.; Di Luzio, E.; Delchiaro, M.; Di Martire, D.; Minnillo, M.; Rouhi, J.; Martino, S.; Della Seta, M.; Troiani, F.; et al. Deep-Seated Gravitational Slope Deformations in Molise Region (Italy): Novel Inventory and Main Geomorphological Features. *J. Maps* **2023**, 1–14. [CrossRef]
- Ietto, F.; Conforti, M.; Tolomei, C.; Cianflone, G. Village Relocation as Solution of the Landslide Risk, Is It Always the Right Choice? The Case Study of Cavallerizzo Ghost Village (Calabria, Southern Italy). *Int. J. Disaster Risk Reduct.* **2022**, *81*, 103267. [CrossRef]
- Pescatore, T.S.; Di Nocera, S.; Matano, F.; Pinto, F.; Amore, O.; Critelli, S.; De Riso, R.; Quarantiello, R.; Senatore, M.R. Note Illustrative della Carta Geologica d’Italia alla Scala 1:50,000—Foglio 419 San Giorgio la Molara. ISPRA – Istituto Superiore per la Protezione e la Ricerca Ambientale. printing. Available online: https://www.isprambiente.gov.it/Media/carg/note_illustrative/419_SanGiorgio_LaMolara.pdf (accessed on 3 April 2023).
- Hung, O.; Leroueil, S.; Picarelli, L. The Varnes Classification of Landslide Types, an Update. *Landslides* **2014**, *11*, 167–194. [CrossRef]
- Peternel, T.; Janža, M.; Šegina, E.; Bezak, N.; Maček, M. Recognition of Landslide Triggering Mechanisms and Dynamics Using GNSS, UAV Photogrammetry and In Situ Monitoring Data. *Remote Sens.* **2022**, *14*, 3277. [CrossRef]
- Wen, T.; Hu, Z.; Tang, H. The Field Survey and Deformation Characteristics of Exit Slope of Qingshuigou Tunnel in the Southwest of China. *Arab. J. Geosci.* **2022**, *15*, 1096. [CrossRef]
- Jia, W.; Wen, T.; Li, D.; Guo, W.; Quan, Z.; Wang, Y.; Huang, D.; Hu, M. Landslide Displacement Prediction of Shuping Landslide Combining PSO and LSSVM Model. *Water* **2023**, *15*, 612. [CrossRef]
- Crippa, C.; Valbuzzi, E.; Frattini, P.; Crosta, G.B.; Spreafico, M.C.; Agliardi, F. Semi-Automated Regional Classification of the Style of Activity of Slow Rock-Slope Deformations Using PS InSAR and SqueeSAR Velocity Data. *Landslides* **2021**, *18*, 2445–2463. [CrossRef]
- Discenza, M.E.; Di Luzio, E.; Martino, S.; Minnillo, M.; Esposito, C. Role of Inherited Tectonic Structures on Gravity-Induced Slope Deformations: Inference from Numerical Modeling on the Luco Dei Marsi DSGSD (Central Apennines). *Appl. Sci.* **2023**, *13*, 4417. [CrossRef]
- Wen, T.; Tang, H.; Huang, L.; Wang, Y.; Ma, J. Energy Evolution: A New Perspective on the Failure Mechanism of Purplish-Red Mudstones from the Three Gorges Reservoir Area, China. *Eng. Geol.* **2020**, *264*, 105350. [CrossRef]
- Novellino, A.; Cesarano, M.; Cappelletti, P.; Di Martire, D.; Di Napoli, M.; Ramondini, M.; Sowter, A.; Calcaterra, D. Slow-Moving Landslide Risk Assessment Combining Machine Learning and InSAR Techniques. *CATENA* **2021**, *203*, 105317. [CrossRef]
- Soltanieh, A.; Macciotta, R. Updated Understanding of the Ripley Landslide Kinematics Using Satellite InSAR. *Geosciences* **2022**, *12*, 298. [CrossRef]

18. Bhattacharya, A.; Mukherjee, K. Review on InSAR Based Displacement Monitoring of Indian Himalayas: Issues, Challenges and Possible Advanced Alternatives. *Geocarto Int.* **2017**, *32*, 298–321. [[CrossRef](#)]
19. Delacourt, C.; Allemand, P.; Berthier, E.; Raucoules, D.; Casson, B.; Grandjean, P.; Pambrun, C.; Varel, E. Remote-Sensing Techniques for Analysing Landslide Kinematics: A Review. *Bull. Société Géologique Fr.* **2007**, *178*, 89–100. [[CrossRef](#)]
20. Donati, D.; Stead, D.; Geertsema, M.; Bendle, J.M.; Menounos, B.; Borgatti, L. Kinematic Analysis of the 2020 Elliot Creek Landslide, British Columbia, Using Remote Sensing Data. *Front. Earth Sci.* **2022**, *10*, 916069. [[CrossRef](#)]
21. Fusco Girard, L.; De Toro, P. Integrated Spatial Assessment: A Multicriteria Approach to Sustainable Development of Cultural and Environmental Heritage in San Marco Dei Cavoti, Italy. *Cent. Eur. J. Oper. Res.* **2007**, *15*, 281–299. [[CrossRef](#)]
22. Bozzano, F.; Esposito, C.; Franchi, S.; Mazzanti, P.; Perissin, D.; Rocca, A.; Romano, E. Understanding the Subsidence Process of a Quaternary Plain by Combining Geological and Hydrogeological Modelling with Satellite InSAR Data: The Acque Albule Plain Case Study. *Remote Sens. Environ.* **2015**, *168*, 219–238. [[CrossRef](#)]
23. Ishwar, S.G.; Kumar, D. Application of DInSAR in Mine Surface Subsidence Monitoring and Prediction. *Curr. Sci.* **2017**, *112*, 46–51. [[CrossRef](#)]
24. Coda, S.; Tessitore, S.; Di Martire, D.; Calcaterra, D.; De Vita, P.; Allocca, V. Coupled Ground Uplift and Groundwater Rebound in the Metropolitan City of Naples (Southern Italy). *J. Hydrol.* **2019**, *569*, 470–482. [[CrossRef](#)]
25. Nof, R.N.; Abelson, M.; Raz, E.; Magen, Y.; Atzori, S.; Salvi, S.; Baer, G. SAR Interferometry for Sinkhole Early Warning and Susceptibility Assessment along the Dead Sea, Israel. *Remote Sens.* **2019**, *11*, 89. [[CrossRef](#)]
26. Bianchini, S.; Confuorto, P.; Intrieri, E.; Sbarra, P.; Di Martire, D.; Calcaterra, D.; Fanti, R. Machine Learning for Sinkhole Risk Mapping in Guidonia-Bagni Di Tivoli Plain (Rome), Italy. *Geocarto Int.* **2022**, *37*, 16687–16715. [[CrossRef](#)]
27. Zeni, G.; Bonano, M.; Casu, F.; Manunta, M.; Manzo, M.; Marsella, M.; Pepe, A.; Lanari, R. Long-Term Deformation Analysis of Historical Buildings through the Advanced SBAS-DInSAR Technique: The Case Study of the City of Rome, Italy. *J. Geophys. Eng.* **2011**, *8*, S1–S12. [[CrossRef](#)]
28. Weissgerber, F.; Colin-Koeniguer, E.; Nicolas, J.-M.; Trouvé, N. 3D Monitoring of Buildings Using TerraSAR-X InSAR, DInSAR and PolSAR Capacities. *Remote Sens.* **2017**, *9*, 1010. [[CrossRef](#)]
29. Nettis, A.; Massimi, V.; Nutricato, R.; Nitti, D.O.; Samarelli, S.; Uva, G. Satellite-Based Interferometry for Monitoring Structural Deformations of Bridge Portfolios. *Autom. Constr.* **2023**, *147*, 104707. [[CrossRef](#)]
30. Cascini, L.; Fornaro, G.; Peduto, D. Advanced Low- and Full-Resolution DInSAR Map Generation for Slow-Moving Landslide Analysis at Different Scales. *Eng. Geol.* **2010**, *112*, 29–42. [[CrossRef](#)]
31. Di Martire, D.; Novellino, A.; Tessitore, S.; Ramondini, M.; Calcaterra, D. Application of DInSAR Techniques to Engineering Geology Studies in Southern Italy. *Rend. Online Della Soc. Geol. Ital.* **2013**, *24*, 97.
32. Ammirati, L.; Di Martire, D.; Bordicchia, F.; Calcaterra, D.; Russo, G.; Mondillo, N. Semi-Real Time Systems for Subsidence Monitoring in Areas Affected by Underground Mining: The Example of the Nuraxi-Figus Coal District (Sardinia, Italy). *Int. J. Coal Sci. Technol.* **2022**, *9*, 91. [[CrossRef](#)]
33. Ren, T.; Gong, W.; Gao, L.; Zhao, F.; Cheng, Z. An Interpretation Approach of Ascending–Descending SAR Data for Landslide Identification. *Remote Sens.* **2022**, *14*, 1299. [[CrossRef](#)]
34. Pescatore, T.S.; Di Nocera, S.; Matano, F.; Pinto, F.; Quarantiello, R.; Ornella, A.; Boiano, U.; Civile, D.; Fiorillo, L.; Martino, C. Geologia Del Settore Centrale Dei Monti Del Sannio: Nuovi Dati Stratigrafici e Strutturali. *Mem. Descr. Carta Geol. It.* **2008**, *77*, 77–94.
35. Vitale, S.; Ciarcia, S. Tectono-Stratigraphic Setting of the Campania Region (Southern Italy). *J. Maps* **2018**, *14*, 9–21. [[CrossRef](#)]
36. Monti, L.; Pescatore, T.S.; Di Nocera, S.; Boiano, U.; Boscaino, M.; Civile, D.; Martino, C.; Matano, F.; Pescatore, E.; Pinto, F.; et al. Carta Geologica d'Italia Alla Scala 1:50,000, Foglio 419 "San Giorgio La Molara" 2010. Available online: https://www.isprambiente.gov.it/Media/carg/419_SANGIORGIO_LAMOLARA/Foglio.html (accessed on 3 April 2023).
37. Sacco, P.; Battagliere, M.L.; Daraio, M.G.; Coletta, A. The COSMO-SkyMed Constellation Monitoring of the Italian Territory: The Map Italy Project. In Proceedings of the 66th International Astronautical Congress IAC, Jerusalem, Israel, 12–16 October 2015; pp. 12–16.
38. Colesanti, C.; Wasowski, J. Investigating Landslides with Space-Borne Synthetic Aperture Radar (SAR) Interferometry. *Eng. Geol.* **2006**, *88*, 173–199. [[CrossRef](#)]
39. Costantini, M.; Ferretti, A.; Minati, F.; Falco, S.; Trillo, F.; Colombo, D.; Novali, F.; Malvarosa, F.; Mammone, C.; Vecchioli, F.; et al. Analysis of Surface Deformations over the Whole Italian Territory by Interferometric Processing of ERS, Envisat and COSMO-SkyMed Radar Data. *Remote Sens. Environ.* **2017**, *202*, 250–275. [[CrossRef](#)]
40. Di Martire, D.; Paci, M.; Confuorto, P.; Costabile, S.; Guastaferro, F.; Verta, A.; Calcaterra, D. A Nation-Wide System for Landslide Mapping and Risk Management in Italy: The Second Not-Ordinary Plan of Environmental Remote Sensing. *Int. J. Appl. Earth Obs. Geoinf.* **2017**, *63*, 143–157. [[CrossRef](#)]
41. Mora, P.; Baldi, P.; Casula, G.; Fabris, M.; Ghirotti, M.; Mazzini, E.; Pesci, A. Global Positioning Systems and Digital Photogrammetry for the Monitoring of Mass Movements: Application to the Ca' Di Malta Landslide (Northern Apennines, Italy). *Eng. Geol.* **2003**, *68*, 103–121. [[CrossRef](#)]
42. Iglesias, R.; Mallorqui, J.J.; Monells, D.; López-Martínez, C.; Fabregas, X.; Aguasca, A.; Gili, J.A.; Corominas, J. PSI Deformation Map Retrieval by Means of Temporal Sublook Coherence on Reduced Sets of SAR Images. *Remote Sens.* **2015**, *7*, 530–563. [[CrossRef](#)]

43. The MathWorks Inc. 'MATLAB'. Natick, Massachusetts: The MathWorks Inc. 2023. Available online: <https://www.mathworks.com> (accessed on 3 April 2023).
44. Bovenga, F.; Pasquariello, G.; Pellicani, R.; Refice, A.; Spilotro, G. Landslide Monitoring for Risk Mitigation by Using Corner Reflector and Satellite SAR Interferometry: The Large Landslide of Carlantino (Italy). *Catena* **2017**, *151*, 49–62. [[CrossRef](#)]
45. Pecoraro, G.; Nicodemo, G.; Menichini, R.; Luongo, D.; Peduto, D.; Calvello, M. Combining Statistical, Displacement and Damage Analyses to Study Slow-Moving Landslides Interacting with Roads: Two Case Studies in Southern Italy. *Appl. Sci.* **2023**, *13*, 3368. [[CrossRef](#)]
46. Guerriero, L.; Prinzi, E.P.; Calcaterra, D.; Ciarcia, S.; Di Martire, D.; Guadagno, F.M.; Ruzza, G.; Revellino, P. Kinematics and Geologic Control of the Deep-Seated Landslide Affecting the Historic Center of Buonalbergo, Southern Italy. *Geomorphology* **2021**, *394*, 107961. [[CrossRef](#)]
47. Intrieri, E.; Frodella, W.; Raspini, F.; Bardi, F.; Tofani, V. Using Satellite Interferometry to Infer Landslide Sliding Surface Depth and Geometry. *Remote Sens.* **2020**, *12*, 1462. [[CrossRef](#)]

Disclaimer/Publisher's Note: The statements, opinions and data contained in all publications are solely those of the individual author(s) and contributor(s) and not of MDPI and/or the editor(s). MDPI and/or the editor(s) disclaim responsibility for any injury to people or property resulting from any ideas, methods, instructions or products referred to in the content.